The International Journal of Advanced Manufacturing Technology (2019) 105:3489–3498
https://doi.org/10.1007/s00170-019-04603-3

ORIGINAL ARTICLE

FEM modeling simulation of laser engraving

Evangelos Nikolidakis[1] · Aristomenis Antoniadis[1]

Received: 3 July 2019 / Accepted: 21 October 2019 / Published online: 12 November 2019

Abstract
In this paper, a 3D simulation model for nanosecond pulsed laser engraving process is developed, using the finite element method (FEM) aiming at the prediction of the final geometry of the workpiece and optimizing the process. A general heat transfer model is adapted where the incidence laser beam causing the material ablation is modeled using a Gaussian surface heat source, taking into account the interaction between the laser beam, the workpiece material, and the generated metal-vapor plasma. To validate the simulation model, a large set of experiments was performed for the purpose of comparing the experimental with the simulation results. The experiments were conducted on stainless steel and a pressure vessel steel plate using the DMG MORI Lasertec 40 machine for various combinations of the three machining process parameters: average power, repetition rate, and scanning speed. The experimental results positively validated the simulation model. The numerical results were examined and some conclusions were drawn about the effect of the machining parameters on the laser engraving process.

Keywords Laser ablation · Laser engraving · Simulation · Finite elements method

1 Introduction

The rapid development of technology in combination with the growing need for the production of new and improved products resulted in innovations and improvements in production methods. One of these was the use of lasers in production methods. Of particular interest is the laser engraving process in microscale, which is now a mature technology with various applications in producing high-tech products for the electronics industry, medical equipment [1] production, telecommunications and automotive, while continuously finding application in new areas.

The basic principle of the laser engraving process is that through laser beam pulses, a large amount of heat is imparted locally into the material of the workpiece that must be removed in order to cause its sublimation. Laser engraving process is based on the laser ablation process of the materials. During the laser ablation process, a laser beam pulse hits the surface of the workpiece material, providing a large amount of focused heat energy first causing melting, then vaporization-ablation and finally the removal of ablated target material in the form of vapor [2, 3]. When a sequence of continuous laser beam pulses is scanned over the workpiece as shown in Fig. 1, the overall ablated material that is removed produces a 3D geometry with a specific thickness, which is called a single pass removed layer. By making multiple passes with a predefined geometry on each layer, 3D geometries are able to be engraved over the workpiece [4]. The way material is removed is influenced by the generated laser beam pulses from the laser machine characteristics (such as the scanning speed V, repetition rate F, average power P, laser beam spot diameter D, and pulse duration t_p) the properties of the workpiece material, and also by the way they interact with each other.

At present, some studies have been carried out modeling the sublimation mechanism during laser drilling [5, 6], laser welding [7, 8], laser cutting [9, 10], laser texturing [11], and laser marking [12] processes but the confirmed studies about modeling and simulating the laser engraving process in 3D geometries are very few. Onischenko et al. [13] created a computer-assisted simulation method for predictive laser beam toolpaths generation for practical 3D geometries. The complete 3D ablated geometry was modeled as a superposition of single-shot craters on a flat surface. The single-shot

✉ Aristomenis Antoniadis
antoniadis@dpem.tuc.gr

1 School of Production Engineering & Management, Micromachining & Manufacturing Modeling Lab, University Campus Kounoupidiana, Technical University of Crete, 73100 Chania, Greece

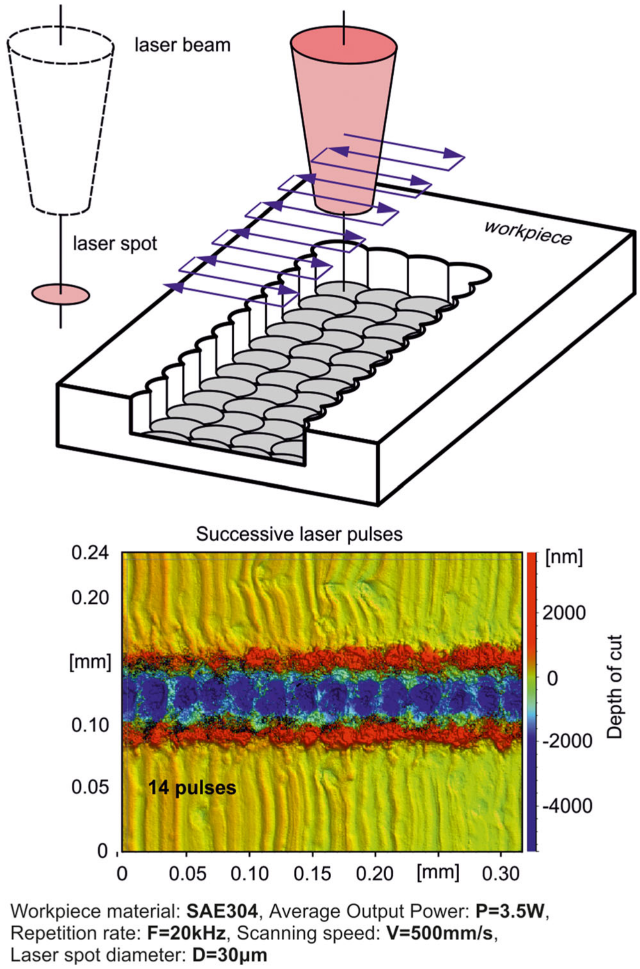

Fig. 1 Schematic presentation of laser engraving process and illustration of the 3D imprint of a series of laser beam pulses on the surface of SAE304 stainless steel plate

crater profile characteristics for different process parameters were taken from experimental data by performing laser ablation process experiments and measuring the craters from the samples using a surface profiler. For the simulation, an initial toolpath was generated using the AlphaCAM software and it was converted into a laser shot map by setting the process parameters. During the simulation, the algorithm modifies the toolpath, the feed rate, and the repetition rate until the simulated shape replicates the requested geometry. The simulation model was tested by ablating 3D structures in a Sol-gel material workpiece and comparing them with requested modeled geometries. Orazi et al. [14] presented a statistical method based on DOE approach that allows the process parameters to be correlated with material removal rate to optimize the process velocity. The advantage of this method over numerical models lies in the fact that a much shorter calculation time is required.

Hamidreza Karbasi [15] performed a computer simulation of the laser engraving process using the commercial finite element method (FEM) software package COMSOL, in order to estimate the depth and the width of an engraved groove. The laser beam was simulated as a moving heat source whose profile was represented by vertical configuration of Hermite-Gaussian mode (TEM01). The simulation was performed for the purpose of moving the laser beam over the surface of the workpiece in a straight line. In order to find the geometry of the engraved groove, the moving mesh technique offered by Comsol was used whereby the geometry mesh was deformed and moved according to user-defined function. Four sets of laser engraving experiments were conducted for steel, aluminum, brass, and copper workpiece materials where the engraved depth and width of the groove were measured and compared with the estimated values from the simulation. Hee Seung Lim and Jeonghoon Yoo [16] made a simulation of the pulsed laser ablation process in nanosecond fields using the finite element method (FEM) commercial package (COMSOL 3.5a). The case of the material ablation caused by a single laser pulse in a two-dimensional (2D) space was examined. The ablation process analyzed the concept of general heat conduction theory where the laser beam absorbed by the material surface is treated as 2D Gaussian heat source. The ablation efficiency for aluminum, copper, steel, and lead materials and various conditions was estimated from the simulation and compared with experimental results given in previous works. Otto et al. [17] created a multiphysical simulation model that allows the simulation of a wide range of laser processes, including laser ablation. The simulation model was built up using the open-source finite volume method (FVM) software package OpenFOAM that is capable of coupling both thermal and fluid dynamical phenomena in the simulation. In the model the laser beam propagation, interaction with the workpiece material, the transition from solid to liquid and from liquid to gas phase, the fluid flow in the melt and the surrounding medium were taken into account. Some test cases were presented and the results from the simulations were compared with the respective values from analytical solutions. Jaeyeol Lee and Jeonghoon Yoo [18] tried to optimize the nanosecond pulsed laser ablation process by performing a simulation using finite element analysis in various cases. Several process parameters such as laser fluence, pulse width, and beam spot size were tested and the results were compared with pre-existing experiments in silicon (Si) material. For the simulation, the classical heat conduction theory was used and it was taken into consideration that the laser beam reflects a 3D Gaussian heat source distribution. A parameter study was carried out to confirm the relation between the process parameters and the results of the simulation. The optimal process parameters of the ablation process were derived using the design of experiments (DOE) methodology. Ren et al. [19]

developed a finite element method simulation model for laser drilling of thin titanium sheets using ANSYS parametric design language (APDL) with life and death technology of the software. The characteristics of the drilled hole such as depth and diameter of the drilled holes predicted by the simulation model were compared with the corresponding values from experiments. Pritamkumar Dake [20] presented a numerical simulation model for pulsed laser ablation process. For the simulation model, into account was taken the interaction between the workpiece material and the laser beam in order to determine the temperature distribution and the ablation depth for multiple successive laser beam pulses. A simulation was performed for a TiC target material using the ANSYS 11 finite element method (FEM) commercial package. Tatra et al. [21] made an extension of the multiphysical model for the simulation of laser ablation processes with short and ultrashort pulses that were previously described in Otto et al. by taking into consideration the difference of the electron and lattice temperature during the ultra-short pulses. Simulations were performed for the ablation process of iron and silicon with pulses in the range of nano and femtoseconds, whose results were compared with existing experimental results.

The aim of this work is the development of a validated 3D finite element simulation model for the nanosecond pulsed laser engraving process. The development of a precise and reliable simulation model is particularly important as it will enable the ability to study the effect of material properties and the process parameters on dimensional accuracy, manufacturing quality, and machining time. In addition, the simulation model will make it possible to perform simulations for various combinations of conditions, process parameters and materials so as to create a database detailing the optimization of the laser engraving process so that the laser machine operator can select the optimal parameters depending on the application.

2 Modeling

Developing a finite element method (FEM) simulation model for laser engraving process is a complicated task because many complex physical processes that have to be modeled happen at the same time. For this reason, the modeling process was split into subprocesses as shown in Fig. 2. At first, the incidence laser beam that is generated from the laser beam machine was modeled. Then a thermal model for the ablation process for a single laser beam pulse in nanosecond fields was developed. Afterward, the material removal mechanism which is caused by the ablation was modeled. Finally, the previous single pulse models expanded for the case of the multiple pulses from a laser map so the laser engraving process for 3D geometries could be modeled.

2.1 Incidence laser beam model

The energy that is needed for heating, melting, and evaporating the material comes from a laser beam pulse that is generated from the laser beam machine. For the incidence laser beam, a heat flux model was used with 2D Gaussian distribution [22] according to the following equation:

$$I_{inc}(x,y) = \frac{2P}{\pi R^2} e^{-2\frac{(x-x_{\mathrm{focus}})^2+(y-y_{\mathrm{focus}})^2}{R^2}} \tag{1}$$

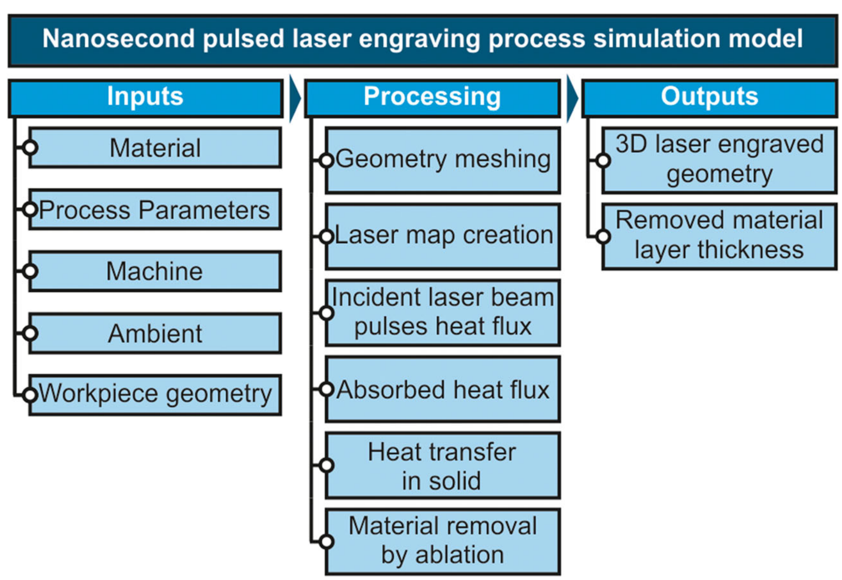

Fig. 2 Presentation of the individual steps to be taken for the laser engraving simulation model

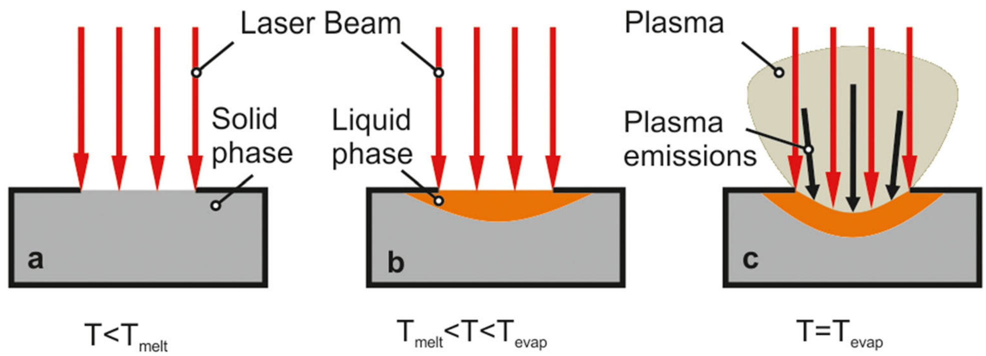

Fig. 3 Ablation process thermal modeling

where I_{inc} is the incidence laser beam heat flux, P is the laser beam power, R is the laser beam spot radius, and (x_{focus}, y_{focus}) are the coordinates of laser beam focus point.

2.2 Ablation process thermal model

The amount of energy that is absorbed from the target material is much lower than the amount of energy that transfers the laser beam as it is generated from the laser beam machine, due to energy losses that take place during the process. In order to examine where the energy losses come from, three cases are demonstrated according to the development stage of the ablation process shown in Fig. 3.

The first case is shown in Fig 3a; the temperature is below the melting temperature and the material is in solid phase. In this instance, only a part of the incidence laser beam irradiance is absorbed from the target material and the rest escapes into the environment. The amount of total power that is absorbed is calculated using the reflectivity coefficient of the material at solid phase, which depends on the target material, the wavelength of the laser beam, and the phase of the material (solid or liquid) as:

$$q_{abs}(x,y) = I_{inc}(x,y)(1-R_{\text{solid}}), T < T_{\text{melt}} \tag{2}$$

where q_{abs} is the absorbed energy flux, I_{inc} is the incidence laser beam heat flux, R_{solid} is the reflectivity of the target material at solid phase, and T_{melt} is the material melting temperature.

In the second case, as shown in Fig. 3b, the target material is in liquid phase which means that the temperature is above the melting temperature but has not reached the evaporating temperature. The amount of the total power that is absorbed is calculated the same way as before using the reflectivity coefficient of the material at melting phase:

$$q_{abs}(x,y) = I_{inc}(x,y)(1-R_{\text{melt}}), \quad T_{\text{melt}} \leq T < T_{\text{evap}} \tag{3}$$

where q_{abs} is the absorbed energy flux, I_{inc} is the incidence laser beam heat flux, R_{melt} is the reflectivity of the target material at liquid phase, T_{melt} is the material melting temperature, and T_{evap} is the material evaporating temperature.

In the third case, as shown in Fig. 3c, the temperature of the target material has reached the evaporating temperature. This means that the target material is in liquid phase but simultaneously material vapor is generated. In this case, a portion of the incidence laser beam irradiance is absorbed by the plume of the material vapor that is above the surface of the target material causing further heating and ionization of the vapor, resulting in the formation of a high-density plasma [23]. The absorption of the incidence laser beam irradiance from the plasma is called laser beam shielding [24]. In the same way as previously described, the amount of the absorbed laser beam power which hits the surface is calculated using the reflectivity coefficient of the material at liquid phase. However, the generated plasma also emits irradiance which hits the target material but only a small amount of it is absorbed and can be calculated using the reflectivity coefficient of the target material for the plasma emission [25]. The following equations describe the phenomena that mentioned before:

$$q_{abs}(x,y) = I_{inc}(x,y)(1-R_{\text{melt}})e^{-a_{pl}*l} + I_P(1-R_P), T = T_{\text{evap}} \tag{4}$$

where $q_{abs}$is the absorbed energy flux, I_{inc} is the incidence laser beam heat flux, R_{melt} is the reflectivity of the target material

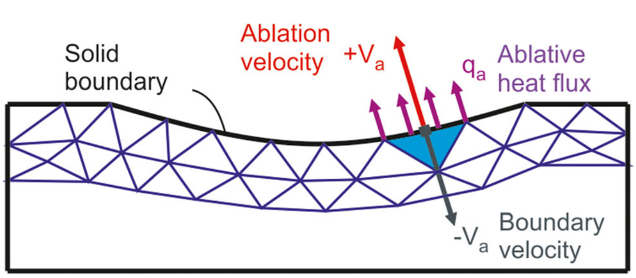

Fig. 4 Material removal by ablation model

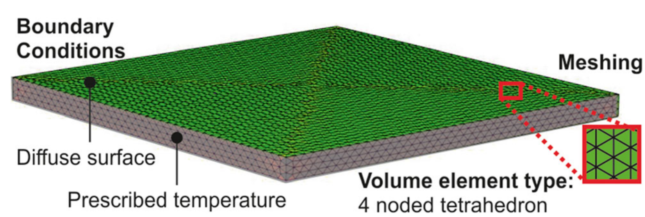

Fig. 5 Mesh model of the workpiece and its boundary conditions

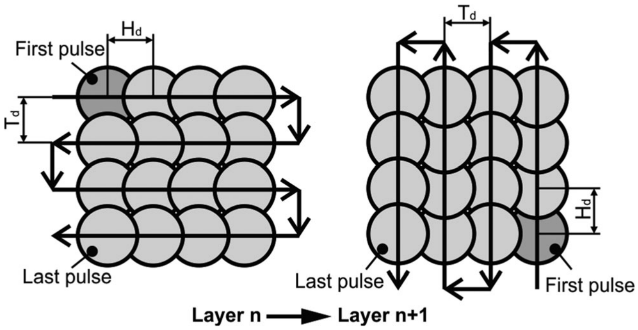

Fig. 6 Laser beam scanning strategy followed by the laser machine and similarly used in simulation model

at liquid phase, a_{pl} is the total absorption coefficient of plasma, l is the thickness of the vapor-material plasma layer, I_P is the irradiance emitted by the plasma, R_P is the target material reflectivity for the plasma emission, and T_{evap} is the material evaporating temperature. The total absorption coefficient of plasma a_{pl} is expressed as:

$$a_{pl} = \sigma_p N \tag{5}$$

where N is atom and ion density during the laser pulse and σ_p is spectral absorption coefficient and expressed as:

$$\sigma_p = 7.9{*}10^{-18}\left(\frac{E_1^*}{h\nu}\right)^3\left(\frac{I_H}{E_1^*}\right)^{0.5} \tag{6}$$

where I_H is the ionization potential of hydrogen, E_1^* is the typical ionization energy of the excited states which can be photoionised, and $h\nu$ is the photon energy. The irradiance emitted by the plasma I_p is expressed as:

$$I_p = \sigma T_P{}^4\left(1 - e^{-a_{pl}{*}l}\right) \tag{7}$$

where σ is the Stefan's constant and T_P is the plasma electron and ion temperature.

2.3 Material removal by ablation model

Since the target material reached the ablation temperature it is transformed to vapor (gas state) and is removed from the domain of interest resulting in a continuous mass transfer and geometry change of the solid boundary. In order to find the frame geometry of the solid body after each step of the finite element analysis, it is sufficient to know the rate at which the solid boundary is ablated. Due to the ablated material removal, an energy transfer occurs between the surface material and the environment called ablative heat flux according to the equation:

$$q_a = \rho H_s v_a \tag{8}$$

where q_a is the ablative heat flux, ρ is the material density, H_s is the heat of sublimation, and v_a is the material ablation velocity which has equal magnitude and opposite direction to the velocity of the solid boundary as shown in Fig. 4.

A thermal boundary condition is used to model the ablation. The ablative heat flux is determined by the following form, satisfying the condition that the temperature of the material cannot exceed the ablation temperature:

Fig. 7 Simulation test results for the case of engraving a 0.12x0.12 mm rectangular pocket with F = 30 kHz, V = 600 mm/s, P = 12 W laser process parameters

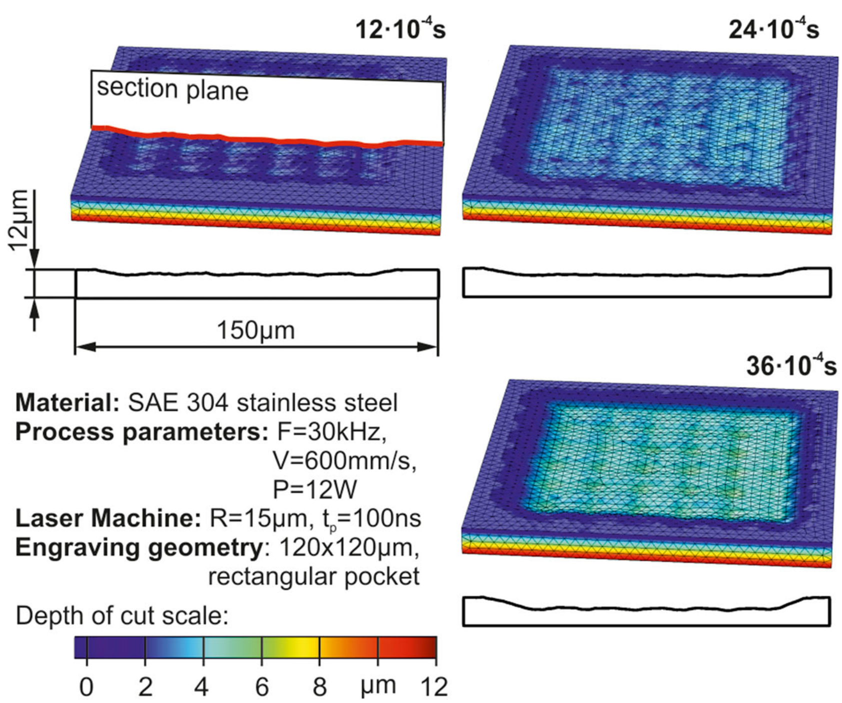

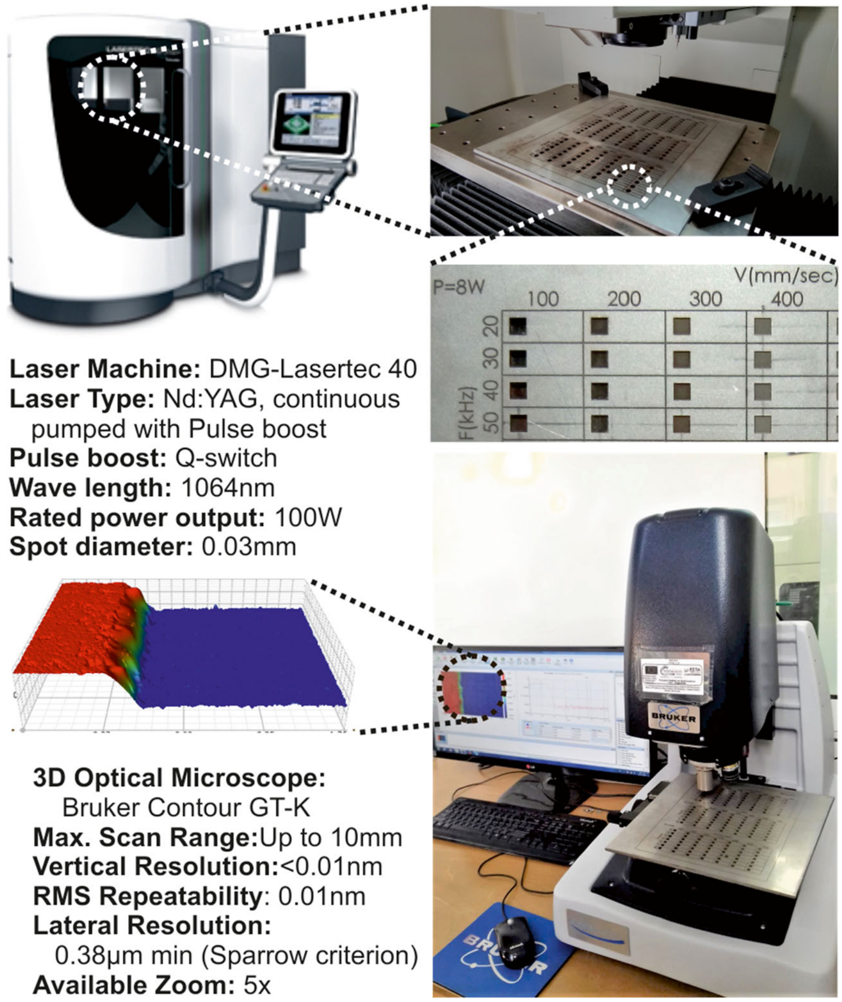

Fig. 8 DMG MORI Lasertec 40 laser engraving machine and Bruker Contoure GT-K 3D optical microscope

$$q_a = h_a(T_a - T) \tag{9}$$

where q_a is the ablative heat flux, T_a is the ablation temperature, and h_a is a temperature-dependent heat transfer coefficient that is zero for $T < T_a$ and increases linearly with a very steep slope for $T > T_a$, in order to ensure that the temperature of the solid cannot exceed the ablation temperature.

From the above equations, the material ablation velocity is calculated, which is equal to the velocity of the solid boundary that is responsible for its deformation. As a consequence, the geometry of the solid boundary is determined.

2.4 Initial-boundary conditions and heat transfer model

The geometry of the 3D solid body that is used for the simulation was set to be a W × D × H rectangular block with the top face to be the target face for the incidence laser beam pulses. As far as the initial and the boundary conditions are concerned, the initial temperature of the solid body T_0 was set to be equal to the ambient temperature $T_0 = T_{amb}$. The top surface that is heated by the laser beam was set to be a diffuse surface (only surface to ambient radiation) and all the other surfaces were considered to have prescribed temperature $T = T_{amb}$ (Dirichlet condition). To model the heat transfer in the solid body, the following version of the heat equation is used:

$$\rho C_p \frac{\partial T}{\partial t} + \nabla \overrightarrow{q} = Q, \quad \overrightarrow{q} = -k \nabla T \tag{10}$$

where ρ is the material density, C_p is the material heat capacity at constant pressure, k is the material thermal conductivity, and Q is the heat source.

2.5 Meshing

For meshing the 3D volume of the simulation, workpiece geometry tetrahedral elements were used. In order to achieve mesh-independent solutions, for the simulation tests, a mesh with maximum element size of 5 μm with denser distribution on the direction of depth was chosen by performing a mesh independence study. This study determines the optimum element size whereby an accurate solution is found at the expense of the least computational resources (Fig. 5).

2.6 Laser map creation

During the laser engraving process, laser beam pulses scan the workpiece material in a predefined way in multiple layers. The complete set of laser beam pulse positions is called laser map. The simulation model is built to generate the laser map in such a way as to have the same characteristics as the laser map that is generated from the DMG MORI Lasertec 40 laser machine software (the machine that was used to perform the experiments for the validation of the model). The scanning strategy was set to cross-hatching as shown in Fig. 6 with track distance T_d (distance between two successive laser beam tracks) to be equal with the hatching distance H_d (distance between two successive laser beam pulses in the same track) which are calculated by the following equation [26]:

$$H_d = \frac{V}{F}, \quad T_d = H_d \tag{11}$$

where H_d is the hatching distance, V is the scanning speed, F is the repetition rate, and T_d is the track distance.

3 Simulation result

Presented in this section is a simulation test that was performed using a simulation workpiece, a 0.15 × 0.15 × 0.012 mm rectangular block of SAE304 stainless steel and process parameters that are shown in Fig. 7. The requested engraved geometry was a 0.12 × 0.12 mm rectangular pocket

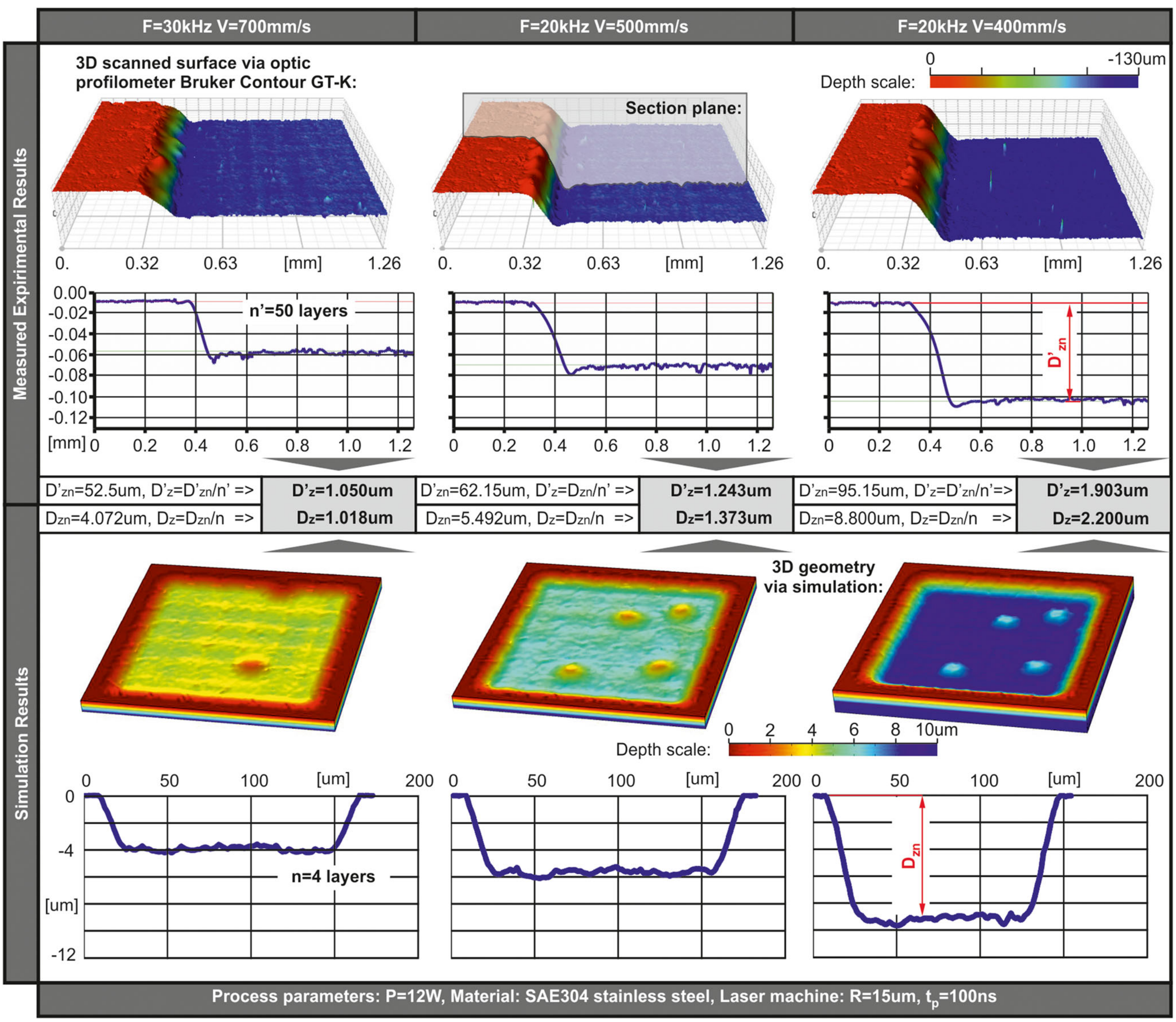

Fig. 9 Measured experimental results compared to simulations results for three cases with different process parameters in each one

made by four-layer laser passes. Through the simulation an estimation of the actual 3D engraved geometry of the pocket was calculated. It showed what would have resulted if the laser engraving process was performed in the same way, with the same material as well as the same process parameters in real conditions.

In Fig. 7, the evolution of the laser engraving process over time is presented, where three snapshots depict the effect of each removed material layer. Moreover, the value of removed material layer thickness D_z was also given as an output from the simulation. It will be used to perform a comparison of the numerical results with the experimental results that are presented below.

4 Experimental results

In order to verify the simulation model, a large set of experiments was performed for the purpose of comparing the experimental with the simulation results. For this purpose, laser engraving process experimental samples were conducted using a DMG MORI Lasertec 40 machine as shown in Fig. 8 for various combinations of the three machining process parameters: average power P, repetition rate F, and scanning speed V. The laser machine was set to generate laser beam pulses with $D = 30um$ spot diameter and $t_p = 100ns$ pulse duration. The sample geometry was a 4 × 4 mm square pocket engraved by a constant number of 50 layers using as workpieces a SAE 304 stainless steel plate (see Fig. 8) and a P355GH pressure vessel steel plate. The scanning strategy was cross-hatching with hatching distance H_d equal to the track distance T_d in the same way used for the simulations.

For each engraved square sample, the hole geometry was scanned using a Bruker Contoure GT-K optic profilometer as shown in Fig. 8 in order to measure the whole engraving depth D'_{zn}. The whole engraving depth D'_{zn} was also measured using the laser machine probing system automated process. The removed material layer thickness D'_z was calculated for each sample by dividing the whole square engraving depth D'_{zn} by the number of layers n' that were performed ($n' =$ 50 in our case). The removed material layer thickness D'_z that came up for each experimental sample is the measured value that will be used for the comparison of the numerical and the experimental results.

5 Model verification

Prediction of the removed material layer thickness D_z is an important task for the laser engraving process because the machine software, given the whole depth of the workpiece to be engraved, is required to decide the number of layers-passes n it will make. The number of layers-passes is calculated by software dividing the whole workpiece depth by the removed material layer thickness. Consequently, the software needs to be given each time the removed material layer thickness for the selected process parameters and the material used. It is worth noting that since there is no prediction tool available at this time, its calculation is carried out by an automated experimental procedure set by the machine manufacturer. However, this procedure is very time consuming and necessarily requires a remnant of the workpiece material to be used for the experimental tests.

A set of laser engraving simulation tests was performed using the same parameters that were used during the laser engraving process of the experimental square pocket samples, in order to be able to perform a comparison between the numerical and the experimental results. For the simulations a 0.15 × 0.15 × 0.012 mm rectangular block of SAE304 stainless steel and P355GH pressure vessel steel respectively was used as workpiece and the requested engraving geometry was a 0.12 × 0.12 mm rectangular pocket made by four-layer passes as shown in Fig. 9. The laser beam spot radius and the pulse duration were set to be $R = 15\ um$ and $t_p = 100\ ns$ respectively so as to be the same with the laser machine-generated beam that was used for the experiments. The removed material layer thickness D_z that was estimated from the simulation and the measured one from the experimental samples is presented in Figs. 10, 11, and 12.

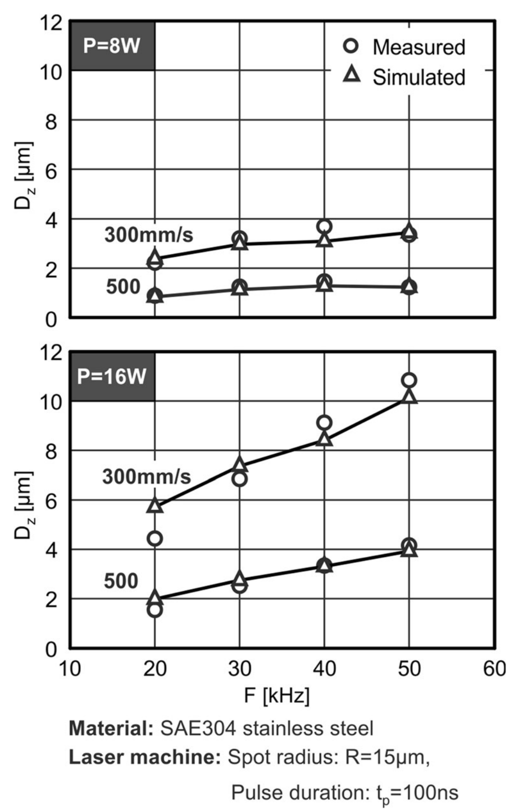

Fig. 10 Removed material layer thickness of SAE304 stainless steel workpiece for $P = 8$ and $P = 16$ W

As shown in Figs. 10, 11, and 12 graphs, there is a great similarity between the simulation results and the experimental ones. The estimated values of the removed material layer thickness D_z are very approximate and have similar tendency with the measured ones from the laser engraving experimental samples. Therefore, by utilizing the numerical results, some conclusions can be drawn about the effect of the machining process parameters on the removed material layer thickness D_z, which are also confirmed by the experimental data. As far as the average power P is concerned, it is observed that the removed material layer thickness D_z increases as the average power P is increased. Regarding the scanning speed V, it is observed that the removed material layer thickness D_z

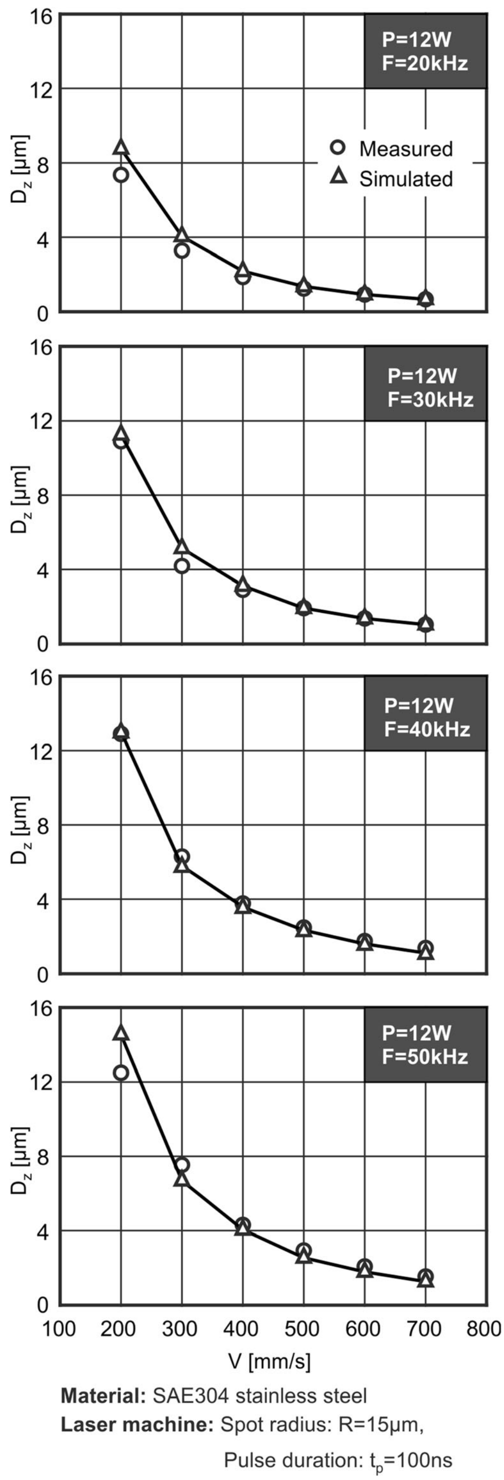

Fig. 11 Removed material layer thickness of SAE304 stainless steel workpiece for P = 12 W

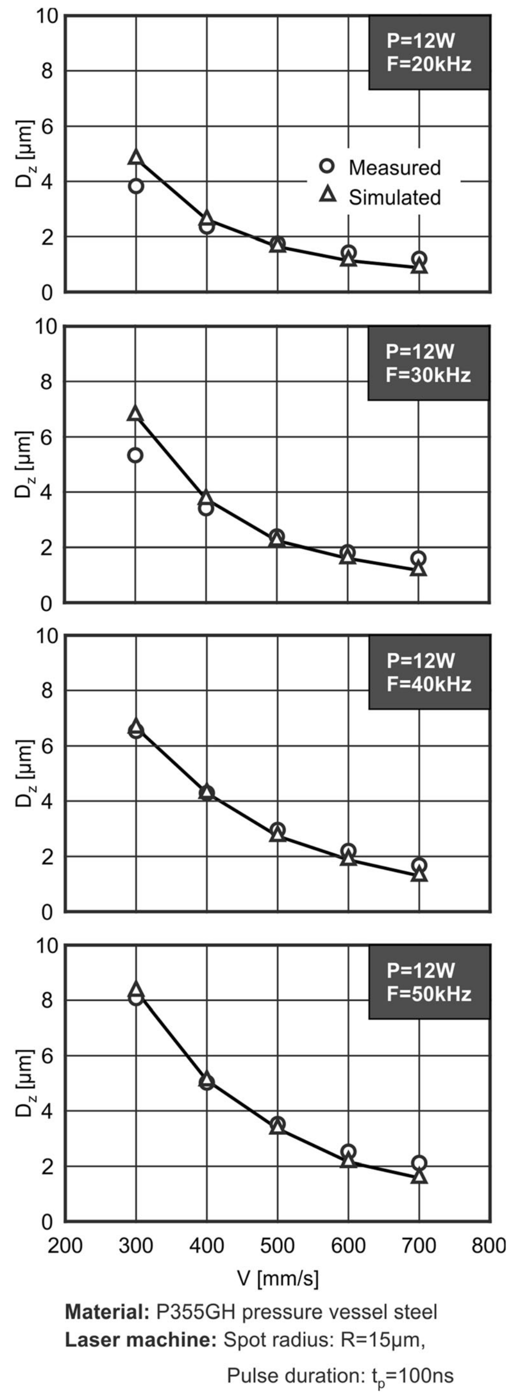

Fig. 12 Removed material layer thickness of P355GH pressure vessel steel workpiece for P = 12 W

increases by decreasing the scanning speed V. Finally, as for the repetition rate F, it is observed that increasing the repetition rate F increases the removed material layer thickness D_z.

6 Conclusions

In this work, modeling of the laser engraving process in nanosecond fields was studied and a 3D finite element simulation model was developed. Considering the machining parameters, the material used and the laser machine characteristics, the simulation model predicts the 3D engraving geometry that would arise if the process was carried out in real conditions. The model was confirmed by comparing experimental values of the removed material layer thickness with the corresponding numeric values derived from the simulations for the engraving of a rectangular pocket. In future work, a database of the results from many simulations for different process parameters, materials, etc., could be created, maintaining values related to the quality of the workpiece such as roughness, thus optimizing the laser engraving process parameters.

Funding information This research is co-financed by Greece and the European Union (European Social Fund- ESF) through the Operational Programme "Human Resources Development, Education and Lifelong Learning" in the context of the project "Strengthening Human Resources Research Potential via Doctorate Research—2nd Cycle" (MIS-5000432), implemented by the State Scholarships Foundation (ΙΚΥ).

References

1. Nour M, Lakhssassi A, Kengne E, Bougataya M (2015) 3D simulation of laser interstitial thermal therapy in the treatment of brain tumors. In: Proceedings of the 2015 COMSOL Conference. COMSOL, Boston
2. Campanelli SL, Ludovico AD, Bonserio C et al (2007) Experimental analysis of the laser milling process parameters. J Mater Process Technol 191:220–223
3. Mladenovič V, Panjan P, Paskvale S et al (2016) Investigation of the laser engraving of AISI 304 stainless steel using a response-surface methodology. TEH VJESN 23(1):265–271
4. Romolia L, Tantussib F, Fuso F (2017) Laser milling of martensitic stainless steels using spiral trajectories. Opt Lasers Eng 91:160–168
5. Sharma S, Pachuary Y, Akhtar SN, Ramkumar J (2015) A study on hydrodynamics of melt expulsion in pulsed Nd: YAG laser drilling of titanium. In: Proceedings of the 2015 COMSOL Conference. COMSOL, Pune
6. Girardot J, Lorong P, Illoul L et al (2017) Modeling laser drilling in percussion regime using constraint natural element method. Int J Mater Form 10(2):1–15
7. He X (2012) Finite element analysis of laser welding: a state of art review. Mater Manuf Process 27:1354–1365
8. Courtois M, Carin M, Le Masson P et al (2013) A new approach to compute multi-reflections of laser beam in a keyhole for heat transfer and fluid flow modelling in laser welding. J Phys D Appl Phys 46:505305 (14 pp)
9. Kim MJ (2005) 3D finite element analysis of evaporative laser cutting. Appl Math Model 29:938–954
10. Sifullah AM, Nukman Y, Hassan MA, Hossain A (2016) Finite element analysis of fusion laser cutting on stainless steel-304. ARPN J Eng Appl Sci 11(1):181–189
11. Ebrahimi Orimi H, Jagadeesh S, Narayanswamy S (2018) Experimental investigation of texturing complex geometry using high repetition nano laser and comparison with the simulated COMSOL model. In: Proceedings of Laser-based Micro- and Nanoprocessing XII LASE 2018. SPIE, San Francisco
12. Wang D, Yu Q, Zhang Y (2015) Research on laser marking speed optimization by using genetic algorithm. PLoS One 10(5): e0126141
13. Onischenko AI, George DS, Holmes AS, Otte F (2004) Efficient pocketing simulation model for solid state laser micromachining and its application to a sol-gel material. In: Proceedings of Photonics West LASE 2004. SPIE, San Jose
14. Orazi L, Cuccolini G, Fortunato A, Tani G (2009) An automated procedure for material removal rate prediction in laser surface micromanufacturing. Int J Adv Manuf Technol 46:163–171
15. Karbasi H (2010) COMSOL assisted simulation of laser engraving. In: In: Proceedings of the 2010 COMSOL Conference. COMSOL, Boston
16. Lim HS, Yoo J (2011) FEM based simulation of the pulsed laser ablation process in nanosecond fields. J Mech Sci Technol 25: 1811–1816
17. Otto A, Koch H, Vazquez RG (2012) Multiphysical simulation of laser material processing. Phys Procedia 39:843–852
18. Lee J, Yoo J (2013) Optimization of the nano-second pulsed laser ablation process using finite element analysis. In: Proceedings of 10th World Congress on Structural and Multidisciplinary Optimization. ISSMO, Orlando
19. Ren N, Jiang L, Liu D et al (2014) Comparison of the simulation and experimental of hole characteristics during nanosecond-pulsed laser drilling of thin titanium sheets. Int J Adv Manuf Technol 76: 735–743
20. Dake P (2015) Numerical simulation of pulse laser ablation. Int J Adv Prod Mech Eng 1(1):84–90
21. Tatra S, Vázquez RG, Stiglbrunner C, Otto A (2016) Numerical simulation of laser ablation with short and ultra-short pulses for metals and semiconductors. Phys Procedia 83:1339–1346
22. Fu CH, Guo YB (2014) 3-Dimensional finite element modeling of selective laser melting Ti-6Al-4V alloy. In: Proceedings of 25th Annual International Solid Freeform Fabrication Symposium. Laboratory for Freeform Fabrication and University of Texas at Austin,Austin
23. Marla D, Bhandarkar UV, Joshi SS (2011) Critical assessment of the issues in the modeling of ablation and plasma expansion processes in the pulsed laser deposition of metals. J Appl Phys 109: 021101
24. Vadillo JM, Fernández Romero JM, Rodríguez C, Laserna JJ (1999) Effect of plasma shielding on laser ablation rate of pure metals at reduced pressure. Surf Interface Anal 27:1009–1015
25. Lunney JG, Jordan R (1998) Pulsed laser ablation of metals. Appl Surf Sci 127–129:941–946
26. Campanelli SL, Casalino G, Contuzzi N (2013) Multi-objective optimization of laser milling of 5754 aluminum alloy. Opt Laser Technol 52:48–56